INNOVATIVE MECHANICAL ENGINEERING **ISSN 2812-9229 (Online)**
University of Niš, Faculty of Mechanical Engineering
VOL. 2, NO 1, 2023, PP. 130 - 143

Original scientific paper *

CFD MODELING TO DETERMINE THE OUTLET WATER JET FORMATIONS AND HYDRODYNAMIC CHARACTERISTICS OF A DAM BOTTOM OUTLET GATE

Filip Stojkovski[1], Sašo Belšak[1], Robert Broz[1], Valentino Stojkovski[2]

[1] Iskra Impuls Slovenia

[2] Faculty of Mechanical Engineering, University SS Cyril and Methodius, N. Macedonia

Abstract. *Multiphase flow modeling using numerical simulation approach is by no means a simple task, especially when defining flow conditions in non-closed domain (such as outflows, spillways and open channel flows), compared to mixing of fluids in tanks or vessels. The task which was done was part of a refurbishment project of a regulating fixed-wheel bonneted gate of a dam bottom outlet works, so to obtain precise values of the hydrodynamic forces acting on the gate, to see if down-pull effect occurs in every gate position. The outflow conditions are in open atmosphere, so the formation of the water jet plays a crucial part to estimate the discharge rate of the bottom outlet. The numerical modeling was made via CFD simulations using the Volume of Fluid model, to gain phase fractions of water and ambient air and to see the water jet formation behind the gate. The obtained results are compared in several ways. The numerically obtained discharge rates for a given reservoir level were compared with the available model test data, dating from the origin of the dam. The numerically obtained hydrodynamic forces, hydraulic cylinder pressures and gate casing cover pressures are compared with physical measured data on site during the wet test of the gate functionality. The obtained jet formations behind the gate were examined through a drone footage taken at the same time when the wet test was made, to evaluate the CFD multiphase modelling approach visually with the real outflow conditions. All the mentioned result comparisons showed remarkable exactness and similarity with the available data, on-site measurements and drone footage, showing that all the steps taken to perform CFD evaluation give great prediction of the overall hydrodynamic conditions occurring on-site.*

Key words: *CFD, Hydraulic Gates, Measurements, Multiphase flow, Volume of Fluid (VOF)*

*__Received: May 24, 2023 / Accepted May 30, 2023.__
Corresponding author: Filip Stojkovski
Iskra Impuls, Slovenia
e-mail: filip.stojkovski@iskraimpuls.si

1. INTRODUCTION

Dams and Hydropower plants in the Balkan region, especially in the countries of Ex-Yugoslavia, are coming to a period where reconstruction works must be considered, to prolong their operational period and to improve their performance. Mainly, reconstruction works on hydraulic gates are not specifically described by any standard and mainly are based on practical experience of the engineers throughout the years of work with this type of hydromechanical equipment. Before estimating the scope of refurbishment works on a hydraulic gate, analytical and numerical calculations are needed to predict the overall situation happening on-site, expected loading situations, hydrodynamic forces, flow rates and outflow conditions, lifting pressures etc.

This paper represents the numerical approach before and after refurbishment works done on a regulating fixed-wheel bonneted gate of a dam bottom outlet works. The numerical approach was made with CFD analysis, to define the hydrodynamic conditions occurring on-site, the hydrodynamic forces acting on the gate and to estimate the flow rates for various gate positions and reservoir water levels. The works were made on the dam bottom outlet regulation gate of HPP Rama in Bosnia & Herzegovina.

Fixed-wheel vertical lifting bonneted gate was installed back in 1967, at the outlet section of the dams' bottom outlet tunnel. The overall size (gate body height, span and depth) is 4.3x3.3x0.75, respectively. At the lower seal, the gate lip is designed with a 45° angle slope. The gate is driven by a hydraulic cylinder mounted on the top of the gate casing cover, directly connected without lifting rods. The total lifting height of the gate is Z_{MAX}=4.2 [m], but the net clearance height of the bottom outlet is Z_0=4[m], forming a 4x1.9 net cross section area. The bottom outlet slope inclination is around +8° where the outflow is in the form of a jet, theoretically as projectile motion. The concrete channel where the jet is formed is with side slopes of 7°, which start immediately after the gate body. The overall situation is given in Fig. 1.

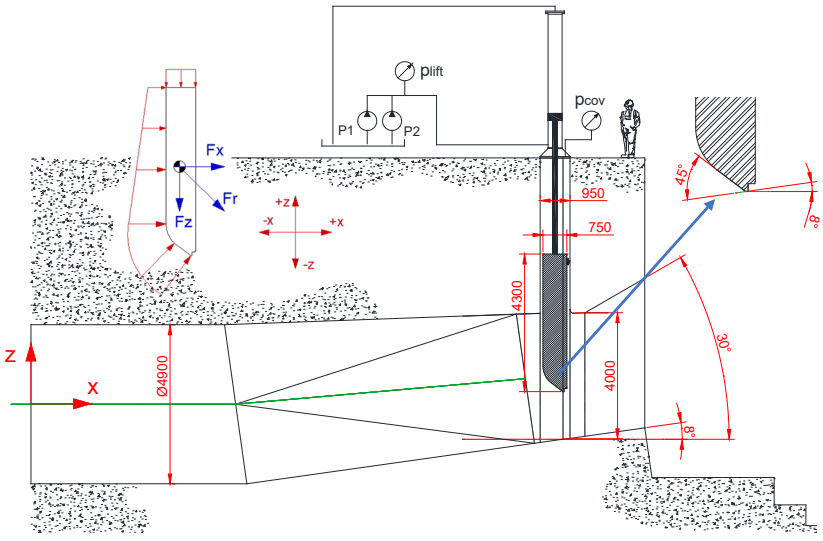

Fig. 1 Schematic of the overall situation at the bottom outlet regulation gate

The gate is driven by using two hydraulic pumps operating in parallel mode, to fulfill the flow rates i.e. the lifting velocity of the gate. The lifting pressure was measured during the tests indicated as p_{lift}, and the pressure on the casing cover was measured and compared with the numerically obtained results, which is indicated as p_{cov} in Fig. 1. Measured values were taken for several gate test positions on site and the numerically obtained results were compared for the same gate positions.

The physics behind the hydrodynamic forces [1] relies on the total pressure (energy) in front of the gate, which is taken as the water level in the reservoir, and the gate position of opening. In the CFD simulations which were carried out and explained in the following context, two major forces were taken into account, i.e. the net horizontal force which pushes the gate towards the wheels and the net vertical force which can develop down-pull or up-lift effect on the gate body. The CFD results give the values of these forces on the gate body, while on-site measurements were made on the lifting pressure of the cylinder, so the measured pressure represents the algebraic sum of the hydrodynamic forces and the resistant forces (wheels and seals frictions) of the gate. The friction forces are analytically calculated according to [2,3], and added on the obtained net forces from the CFD analysis, to compare them with the measured lifting pressures. For a gate position Z_G $[m]$, the change of the friction in the seals is:

$$F_{\mu s} = f(H_W, Z_G, q_{ss}, \mu_{ss}) \tag{1}$$

where H_W is the head in front of the gate, Z_G is the gate position, q_{ss} is the pre-compressive load on a gate seal and μ_{ss} is the gate seals friction coefficient. As the gate rises, the pressure on the seals decreases and the friction force reduces. The friction of the wheels depends from the net horizontal force on the gate for each gate position, represented as:

$$F_{\mu wh} = f(F_X, Z_G, \mu_1, \mu_2) \tag{2}$$

where F_X is the net horizontal force on the gate from CFD results, and μ_1 and μ_2 are friction coefficients between the wheel and the rolling track and the wheel axle and roller bearings, respectively [2]. Considering the gate weight, noted as $G_G = 200$ $[kN]$ and the friction forces, the lifting force is calculated as:

$$F_{LIFT} = G_G + F_{\mu s} + F_{\mu wh} \pm F_Z \tag{3}$$

where $\pm F_Z$ is the net vertical force on the gate, with the $\pm$ sign depending on the force up-lift or down-pull effect (the force is downwards and pulls the gate towards closing, or the force is upwards and pushes the gate towards opening). The lifting pressure is represented as the lifting force acting on the internal area of the piston and rod of the hydraulic cylinder, and later compared with the measured values on-site. The gate performs self-closure (gravity closure) and cut-off the full flow rate. A good old practice is that regulating gates has a top seal which has full contact with the sealing wall for the whole path of gate movement. This increases the down-pull effect on the gate and the security to obtain a gravity closure of the gate.

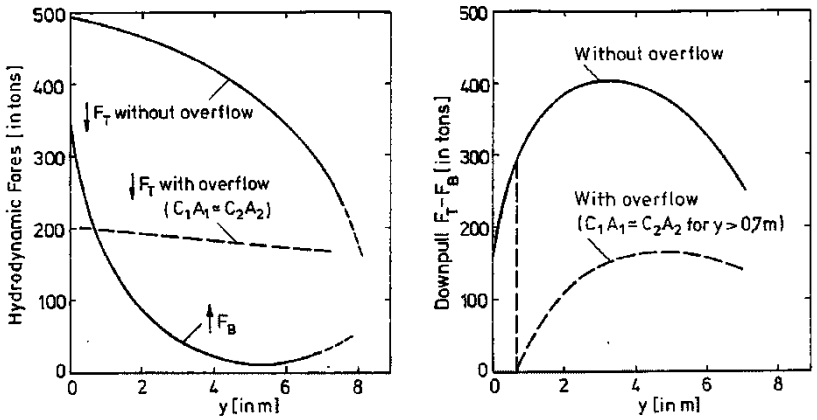

Fig. 2 Down-pull forces on gates with and without overflow (full-contact top sealing) [1]

The results obtained from the CFD analysis for the flow rates are compared with the available model tests data, because on-site flow measurements were unable to be performed. The bottom outlet tunnel is composed of an inlet gate, a tunnel with Ø4900 steel liner with a length of approx. 400 [m] up to the analyzed outlet gate.

2. NUMERICAL MODELING

The numerical simulations were made on a true scale model of the bottom outlet gate of the dam. The simulations were made in Ansys Fluent. The numerical mesh was made in the Fluent Mesher, by using the Watertight meshing technique with Polyhedral mesh, suitable, low cell numbered and adequate with low skewness and high accuracy for numerical computing, to capture the tight regions between the gate and the bonnet. The outflow region was modeled similarly to the real conditions on-site. A circular section of the bottom outlet steel liner was partially modeled, to reduce the numerical domain. This is explained further in section 2.2.

2.1 Multiphase Flow Modeling Approach

To obtain water jet formations behind the gate, multiphase flow modeling is needed, as the flow behind the gate is characterized as water jet forming and dispersing into the ambient air. In multiphase flow, a phase can be defined as an identifiable class of material that has inertial response to and interaction with the flow and the potential field in which it is immersed [9]. A phase is defined as one of the states of the matter; in this case, two phases are considered – air and water. Multiphase flow is the simultaneous flow of several phases, so this multiphase flow modeling is a two-phase flow situation. As the two phases are interpenetrating between each other, the Euler-Euler Volume of Fluid (VOF) approach of multiphase modeling was used, which represents a surface-tracking technique applied to a fixed Eulerian mesh, suitable for two or more immiscible fluids where the position of the interface between the fluids is of interest, such as the water jet – ambient air separations. In the VOF model, a single set of momentum equations is shared by the fluids, and the

volume fraction of each of the fluids in each computational cell is tracked throughout the domain. This is suitable for predicting jet breakup, motion of liquid after a dam break, free surface flows, and steady or transient tracking of any liquid and gas interface [4].

The VOF formulation relies on the fact that two or more fluids are not interpenetrating [4]. For each additional phase in the model, a variable is introduced: the volume fraction of the phase in the computational cell. The fields for all variables and properties are shared by the phases and represent volume-averaged values, when the volume fraction of each of the phases is known at each location. Thus, the variables and properties in any given cell are either purely representative of one of the phases, or representative of a mixture of the phases, depending upon the volume fraction values. The tracking of the interface between the phases is accomplished by the solution of a continuity equation for the volume fraction of one of the phases:

$$\frac{1}{\rho_q}\left[\frac{\partial}{\partial t}\left(\alpha_q \rho_q\right) + \nabla \cdot \left(\alpha_q \rho_q \overrightarrow{v_q}\right) = S_{\alpha_q} + \sum_{p=1}^{n}\left(\dot{m}_{pq} - \dot{m}_{qp}\right)\right] \tag{4}$$

where $\dot{m}_{qp}$ is the mass transfer from phase q to phase p, and, vice-versa $\dot{m}_{pq}$. In the modeled case, the right-hand side of the equation is not applicable, as mass transfer mechanism is not present. So, the volume fraction inside a cell of the mesh is computed for the secondary phase (the driving phase - water) starting as:

$$\sum_{q=1}^{n} \alpha_q = 1. \tag{5}$$

If $0 < \alpha_q < 1$, it indicates an interface between the phases. Using the implicit scheme, a solution was made simultaneously for the phase continuity equation, iteratively together with momentum and pressure. In a two-phase system, indexed 1 and 2 for the primary and secondary phase respectively, where the second phase is the driving phase, the calculated density and viscosity in each cell is:

$$\rho = \alpha_2 \rho_2 + (1 - \alpha_2)\rho_1 \; ; \; \mu = \alpha_2 \mu_2 + (1 - \alpha_2)\mu_1. \tag{6}$$

All other physical properties are calculated in the same manner. A single momentum equation is solved throughout the domain, and the resulting velocity field is shared among the phases. The continuity and momentum equation of the mixture of phases are respectively written as:

$$\frac{\partial}{\partial t}(\rho \vec{v}) + \nabla \cdot (\rho \vec{v}) = S$$

$$\frac{\partial}{\partial t}(\rho \vec{v}) + \nabla \cdot (\rho \vec{v}\vec{v}) = -\nabla p + \nabla \cdot [\mu(\nabla \vec{v} + \nabla \vec{v}^T)] + \rho \vec{g} + \overrightarrow{T_\sigma} \tag{7}$$

which are dependent from the volume fractions of the phases thorough the density and viscosity from Eq.6. Based on the local value of α_q, the appropriate properties and variables are assigned to each control volume within the domain.

The fraction interface modeling is adopted as “Sharp” between the water and air, calculated with the “Compressive Interface” capturing scheme, suitable for “Steady-State Implicit” solutions with “Implicit Body Force” formulation. Energy equation was not included in the analysis, as heat transfer and physical properties of the ambient air (compressibility) are negligible. The surface tension between the phases is negligibly

small, but physically it is present, and it was taken as $0.072\ [N/m]$ set as continuum surface force between the air and water.

2.2 Multiphase Flow Modeling Approach

The numerical domain with the boundary conditions is given in Fig. 3. It is consisted of a segment of the inlet steel liner from the bottom outlet, a reducer, the gate body within the bonnet, the terrain slope and the ambient volume. The operating pressure was set as the atmospheric pressure of $p_{atm} = 101325\ [Pa]$ and the gravity was enabled vertically as $g_Z = -9.81[m/s^2]$.

At the inlet, a total pressure was designated as the water level in the accumulation, where the level is $H_W = 63.76[m]$ or $p_{inlet} = 624311\ [Pa]$. At the inlet in front of the gate, the secondary (driving) phase was imposed as 100 [%] water presence. The outlet sections are represented with the pressure outlet boundary conditions. On the top of the domain was given a static pressure outlet with 0 [Pa] intensity, with imposed primary phase (air) of 100 [%]. On the left, right and front side of the outlet domain, the pressure outlet boundary condition was imposed, with enabled Open-Channel condition, giving a negligible small free surface water level of 1 [m], to address that it represents an outflow of the secondary phase (water). As it was mentioned, the numerical mesh was developed as Polyhedral mesh. The model consists of approx. 600.000 cells. The Fluent Mesher algorithm is automated. The starting conditions of the mesh generation were given from the gate body (lower gate lip) as a fixed size cells, to expand with a 20% increment towards the largest cell. The boundary layer near the walls was determined with 4 cells, with mutual rise of 20%.

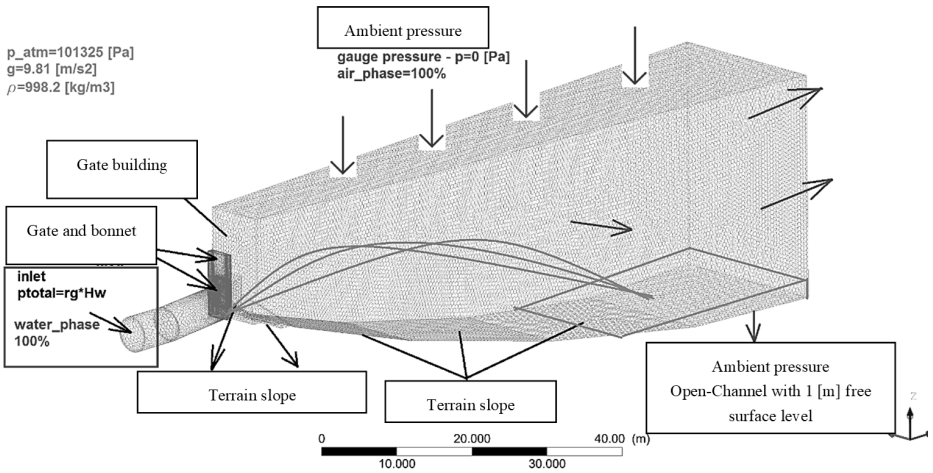

Fig. 3 Numerical domain and boundary conditions

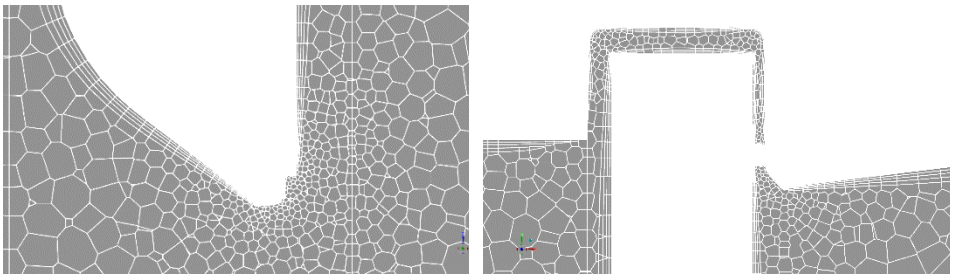

Fig. 4 Numerical mesh example near the gate lip and bonnet

The adopted turbulence model was Standard *k-ε*. The Coupled solver was enabled, coupled with the Volume Fractions, and Pseudo-Transient mode was activated to solve the Navier-Stokes equations. Although the simulations are guided as Steady State, the Pseudo-Transient mode gives a false time step for the solution, for better convergence when volume fractions between phases is present, and the case final solution is representing a Steady State solution. The convergence of residuals reached the value of 10^{-5}.

3. CFD RESULTS

In this section, the pure CFD results are presented, while in the following chapter 4, the comparisons with the measurements were carried out. In this chapter, the water jet formations behind the gate are examined and compared with drone footages from the on-site performed tests. Unfortunately, the footage took place up to 50 [%] of the gate opening, so the results are compared for the positions of the gate up to that point. From the comparisons, it was concluded that there is good match between the CFD results and the footages, so the following gate openings from 50-100% were numerically established, as to see eventual other effects of the jet formation for other operating conditions.

The net hydrodynamic forces are presented in Figs. 5 and 6. One can see that the horizontal force decreases with the gate opening, as the gate is retracted into the bonnet and the flow rate increases. This influence on the decrease of the friction forces from the wheels and the gate seals. The trend is almost linear up to 75[%] of the gate opening, and afterwards, the characteristics drops as the gate is retracted into the bonnet where “dead” static pressure is present (the gate is not influencing the flow stream).

The vertical force which creates the down-pull effect, reaches its optimum between 50 and 65 [%] of the gate opening, showing a tendency to pull the gate downwards. The trend of the curve follows the theoretical curve from Fig. 2, so the simulations show good correspondence with the expected behavior.

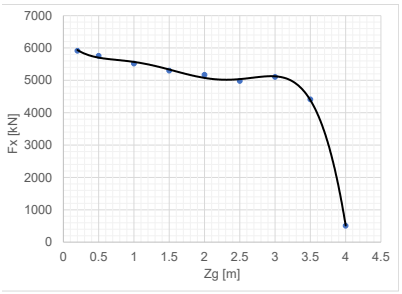

Fig. 5 Horizontal force FX acting on the gate (Drag resistance)

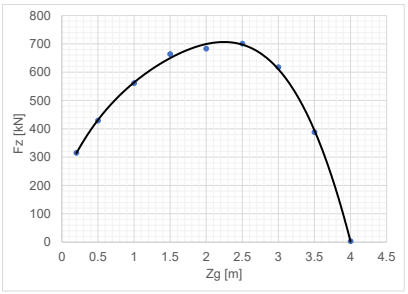

Fig. 6 Vertical force FZ acting on the gate (Down-pull effect)

A pure water jet is hard to be examined, because the true nature of the outflow represents a mixture of the water-air phases (spraying and non-interpenetrating of the phases), shown as water dispersion in the ambient. The following figures show captured sequences from 0-50[%] of the gate opening compared with drone footage images, for the same operating conditions. The on-site footage angle differs from the CFD representation of the results, but clearly shows the jet phenomena which occur and can be easily compared with the CFD obtained results, through the type, length and shape of the jet.

Fig. 7 Z_G=1.25 [%] Opening

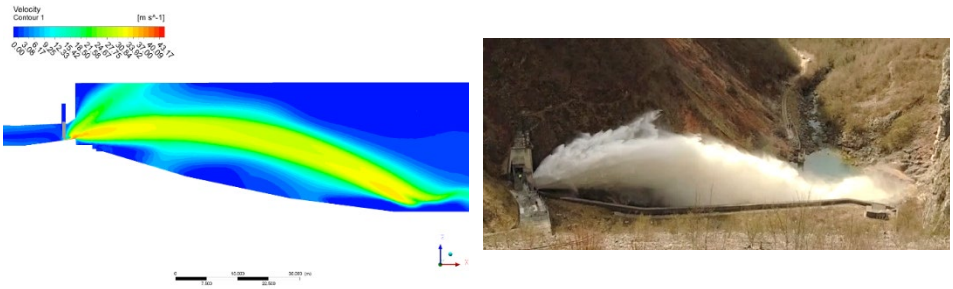

Fig. 8 Z_G=2.5 [%] Opening

From Figs. 7 and 8, one can see that for these partial operating conditions, the CFD obtained water jet forming behind the gate match the on-site conditions. Beside the main water flow beneath the gate, a spray jet is formed, which originates from the corner flow created from the gate position and the clearance.

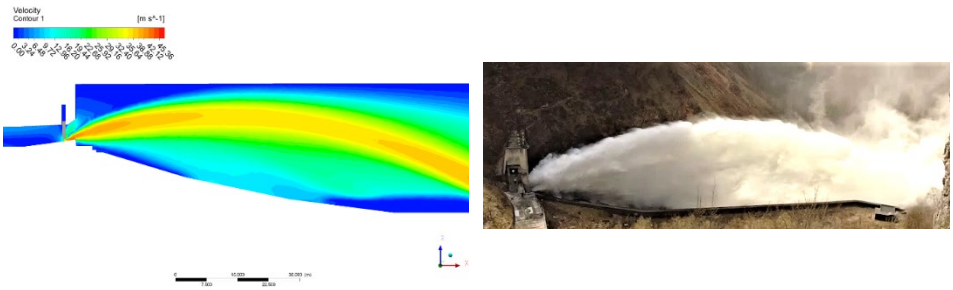

Fig. 9 Z_G=12.5 [%] Opening

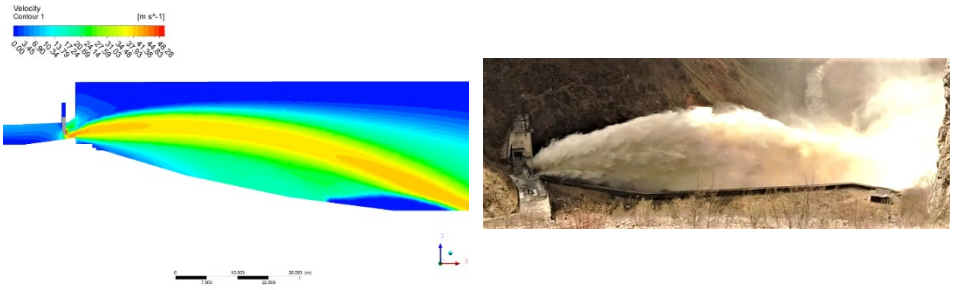

Fig. 10 Z_G=25 [%] Opening

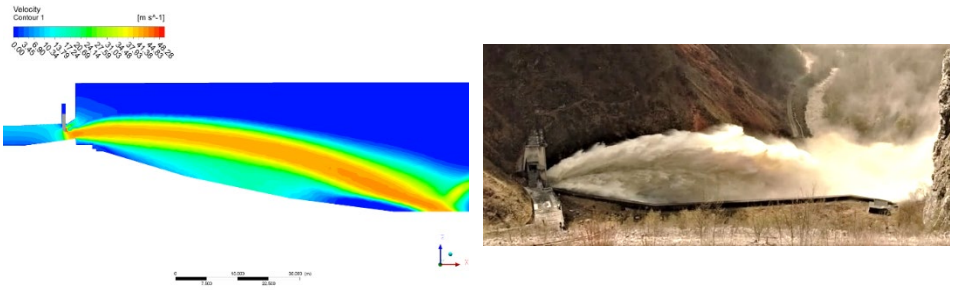

Fig. 11 Z_G=50 [%] Opening

From Figs. 9 to 11, one can see that with satisfactory match, the CFD solution of the water jet formation corresponds with the on-site footages. As the gate travels towards 50 [%] of its opening position, the water jet mainly behaves as non-pure jet, spraying, which

characterizes with a full range and an increased hump. The following operating conditions were not captured with a drone footage. Following these results matches, an assumption has been made the numerical solution, at first sight, visually satisfies the on-site operating conditions. The following gate positions were examined to show the behavior of the water jet formation above 50 [%] opening.

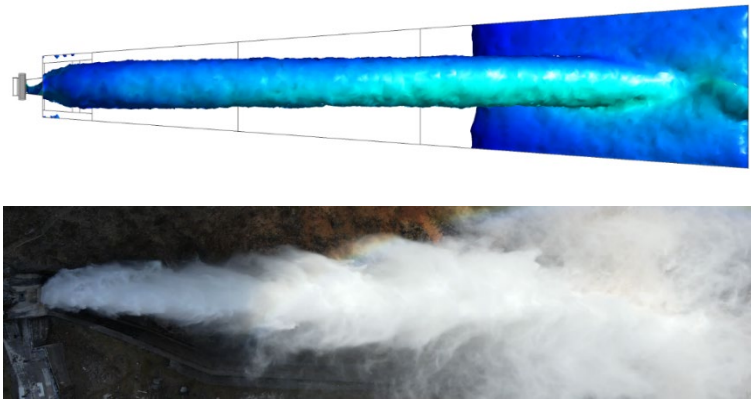

Fig. 12 Z_G=50 [%] Opening – Top view (Water / air interface – 1 [%] water in cells)

A capture of the of the water jet was made at 50 [%] of the gate opening. One can see that the length of the jet matches the on-site footage, but the spread of the jet is mismatched. A dilemma arises that the numerical domain might be too "tight" to capture the spreading of water in the ambient air, where, on the other hand, does not influence the quantitative results.

The following gate openings are analyzed from 50-100 [%] to examine the jet behavior. In Fig. 13, for 62.5 [%] of the gate opening, a shrinkage (shortening) of the jet was obtained, by increased flow rate. Explanation of this phenomenon lies in the geometry of the gate. For fixed-wheel vertical lifting bonneted gates with angled gate lip, as in this case, a "hydrodynamic optimum" (Fig. 6) occurs between the lift and drag force of the immersed gate body, evoking a choke on the flow stream. Between 50 and 65 [%] it is generally known that the maximal down-pull force occurs, i.e. the gate body limit in the influence on the flow stream.

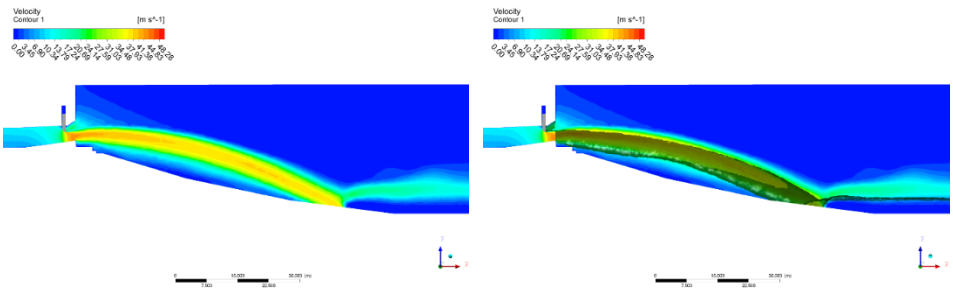

Fig. 13 Z_G=62.5 [%] Opening

Afterwards, in Fig. 14, one can see that when the gate passes the region of 50-65 [%], the jet formation is purer, characterized with full range. An image of the water/air mixture velocities is shown with 1[%] of the water volume fraction.

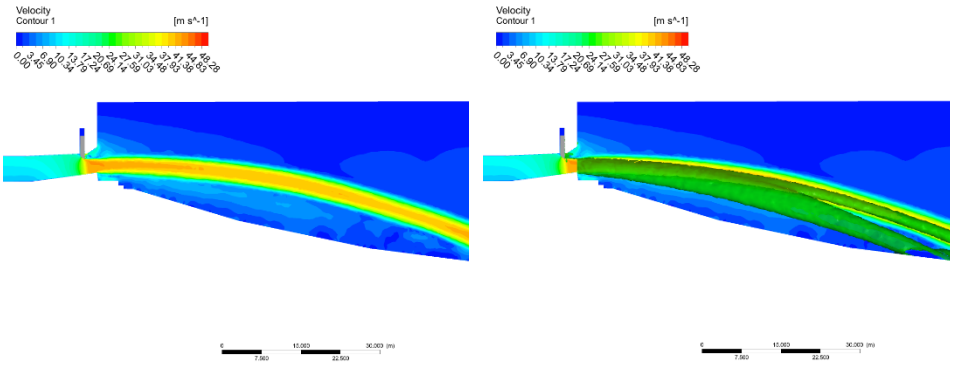

Fig. 14 Z_G=75 [%] Opening

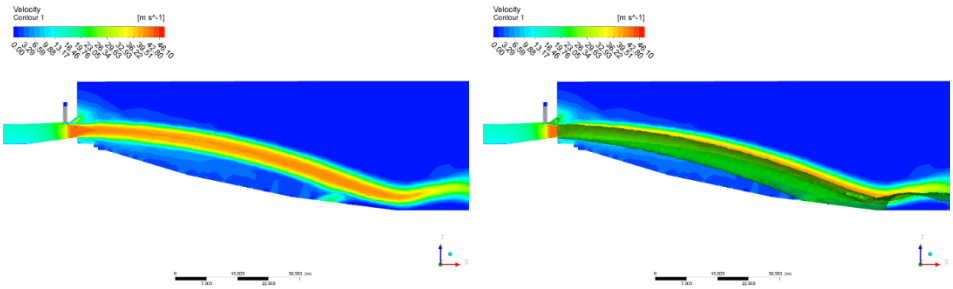

Fig. 15 Z_G=87.5 [%] Opening

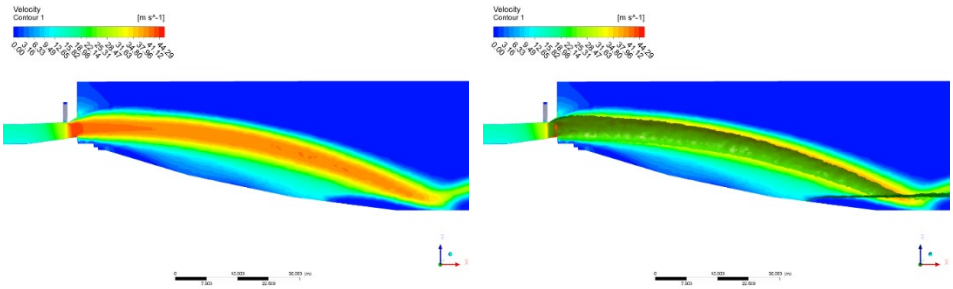

Fig. 16 Z_G=100 [%] Opening

4. EXPERIMENTAL VALIDATION

Observing the water jet formations which corresponds with the footage, and the net forces obtained from the CFD results which corresponds with the theory, friction forces were applied, which were described with Eqs.1 and 2, to obtain close relation with the lifting pressures on-site. Measurements were made on the gate, for the lifting pressure needed for partial gate positions, and the pressure on the casing cover. The measured data is shown with red markers, while the CFD obtained results are shown with a solid blue curve.

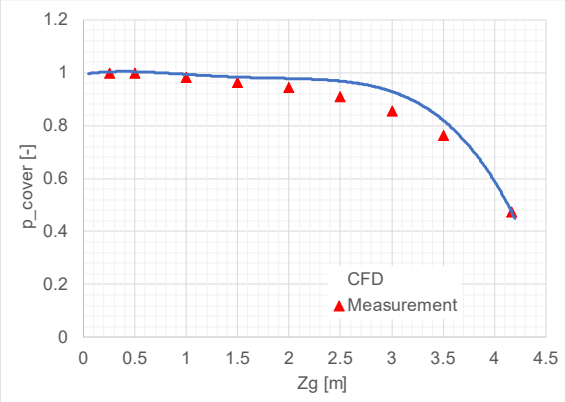

Fig. 17 Pressure on the casing cover - Comparison

In Fig. 17, one can see that a good comparison between the numerically obtained pressures and measured data is achieved on the casing cover, where the numerically obtained results follow the descending trend of the pressure, as the gate opens. In Fig. 18, the CFD results are shown with the measured values for the lifting pressures in the hydraulic cylinder, where good match is achieved. The measured data is shown with red markers, while the CFD obtained results are shown with a solid blue curve.

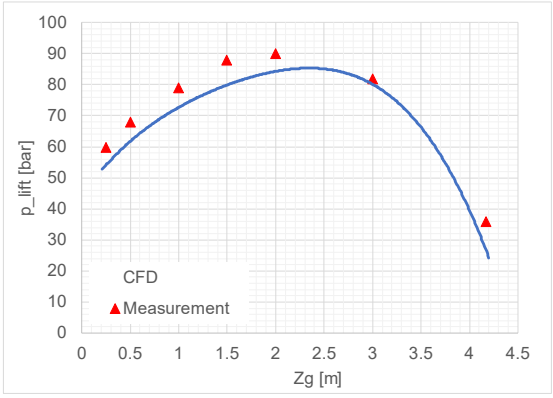

Fig. 18 Gate lifting Pressure - Comparison

The flow rates obtained via CFD simulations were compared with the available data from the model tests, where good match is obtained up to 87.5 [%] of the gate opening (Fig. 19). The maximal flow rate for full gate opening was estimated at 205 [m^3/s]. CFD simulations show a saturation point for the flow rate for maximal gate opening, which shows the influence of the gate on the flow stream. When the gate fully retracts into the bonnet, non-linear point is obtained which represent the flow rate capacity of the bottom outlet without the influence of the gate. The model tests data is shown with red markers, while the CFD obtained results are shown with a solid blue curve.

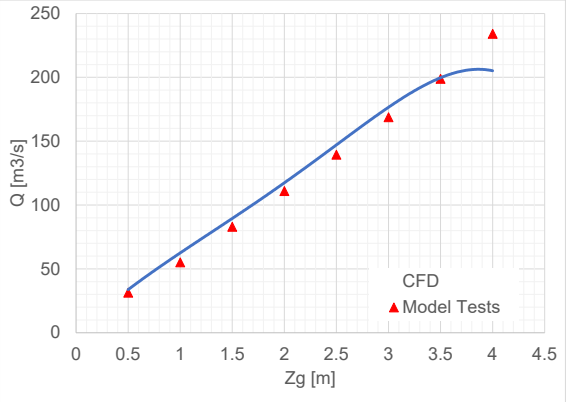

Fig. 19 Flow rates – Comparison with model test data

5. CONCLUSIONS

In this paper, an approach was derived towards modeling the outflow water jet formations behind a dam bottom outlet regulation gate with CFD and it was compared visually and quantitatively with on-site footages and measurements. Using the multiphase volume of fluid approach, good predictions of the water jet formations were obtained which corresponds with the on-site drone footages made. The gate influences the flow stream and the jet formation up to 50 [%] of its opening position, creating non-pure jet, with spraying formations originating from the gate edges with the clearance opening below the gate (vortices, etc.). All the obtained results show good match with the measured values and the available data, for the given water level in the reservoir. This shows that the established CFD approach satisfies the quantitative values of the needed results, but the domain shrinkage could influence the obtained geometry of the water jet formations. Nevertheless, a good approximation was made to predict the hydrodynamic behavior of the gate, before on-site test measurements are carried out, to ensure that the gate can perform well.

The net forces obtained from the simulations were re-defined using the analytical approach with the friction forces from the gate seals and wheels, to achieve approximations with the lifting pressures. Simulation with the applied corrections for the frictions, showed good correspondence with the on-site measured lifting pressures. For additional control, the static pressure was estimated on the casing cover and compared with measured values

on-site, where also a good match was achieved, i.e. the descending trend of the pressure was achieved as the gate lifts.

This shows that the steps taken towards numerical modeling of this type of situations satisfies the needed parameters. It enables a good prediction of the overall situation, which can lead to more firm conclusions when on-site tests and refurbishment works are needed. This approach can be used as a guide for future engineers in the branch of hydromechanics, and it can be implemented before every refurbishment work to predict the behavior of the gate, and can lead to avoiding of undesired situations, which can occur on-site.

REFERENCES

1. Naudascher E., 1991. Hydrodynamic Forces, University of Karlsruhe, Germany.
2. DIN19704, 2004. Hydraulic Steel Structures.
3. Erbisti P.C.F.,2014. Design of Hydraulic Gates, 2nd edition, CRC Publishers.
4. Fluent 6.3 User's Guide.
5. Badas M. et al., 2020. May a Standard VOF Numerical Simulation Adequately Complete Spillway Laboratory Measurements in an Operational Context? The Case of Sa Stria Dam, Water 2020, 12, 1606; doi:10.3390/w12061606.
6. Denner F. Compressive VOF method with skewness correction to capture sharp interfaces on arbitrary meshes.
7. Hui D. Comparison with different interface capture schemes based on gradient smoothing method using unstructured meshes.
8. Viti N., 2019. Numerical simulations of Hydraulic Jumps. Part 2: Recent Results and future work, Water 2019, 11, 28; doi:10.3390/w11010028.
9. Awad M.M. Two-Phase Flow, http://dx.doi.org/10.5772/76201.
10. Brennen C., 2005. Fundamentals of Multiphase Flows, CALTECH.
11. Muralha A., 2020. Assessment of CFD solvers and turbulent models for Water Free Jets in Spillways, Fluids, 5, 104; doi:10.3390/fluids5030104.